Unconventional transport and superconducting properties in electron-doped cuprates

Y. Krockenberger,[1,*] H. Yamamoto,[1] A. Tsukada,[1,†] M. Mitsuhashi,[1,‡] and M. Naito[2]

[1]*NTT Basic Research Laboratories, NTT Corporation, 3-1 Morinosato-Wakamiya, Atsugi, Kanagawa 243-0198, Japan*

[2]*Department of Applied Physics, Tokyo University of Agriculture and Technology Naka-cho 2-24-16, Koganei, Tokyo 184-8588, Japan*

(Received 1 February 2012; published 2 May 2012)

We report a study of transport and magnetic properties of high-quality c axis-oriented superconducting T′-$RE_{2-x}Ce_xCuO_4$ (RE = La, Pr, Nd) thin films grown by molecular beam epitaxy at optimal as well as x = 0.00 doping levels. While the superconducting coherence length ξ_{GL} decreases from RE = Nd to La, it remains nearly constant as a function of doping. For optimally doped T′-cuprates, the electronic conductivity is higher than the dopant-free sample, while T_c is higher for the dopant-free samples for RE = Nd and Pr. We estimated the superconducting penetration depth λ_{ab} by using a relationship obtained from optical measurements and compared it to the diamagnetic response, which corresponds to the superfluid density n_s. Our data suggest that electron doping increases the superfluid density n_s significantly, but the pairing interaction is not affected. In the normal state, the temperature dependence of the resistivity was used to deduce the Fermi temperature T_F, from which we estimated the charge-carrier concentration n. A systematic relationship between n, n_s, and the superconducting transition temperature T_c was not observed. We finally conclude that the superconducting ground state is merely influenced by Ce doping with respect to T_c and ξ_{GL} but solely by the RE element.

DOI: 10.1103/PhysRevB.85.184502 PACS number(s): 61.05.cm, 61.05.jh, 61.72.jj, 66.30.je

I. INTRODUCTION

Superconductivity is one of the most intriguing phenomena in solid-state physics. Particularly, cuprate superconductors show high superconducting (SC) transition temperatures (T_c) and their electronic phase diagram includes a variety of magnetic and electronic interactions. The CuO_2 planes, which are responsible for high-T_c superconductivity, may be doped by either holes or electrons. So far, the majority of research efforts have been spent on hole-doped materials although the understanding of their electron-doped counterparts is essential for obtaining a universal picture of high-T_c superconductivity. The electronic phase diagram of cuprate superconductors compares hole- and electron-doped cuprates. $La_{2-x}Sr_xCuO_4$ is typically used as a representative for the hole-doped side, whereas $Nd_{2-x}Ce_xCuO_4$ for the electron-doped side due to their stoichiometric similarities. Both, $Nd_{2-x}Ce_xCuO_4$ and $La_{2-x}Sr_xCuO_4$, crystallize in the tetragonal space group $I4/mmm$. In the case of $La_{2-x}Sr_xCuO_4$, Cu is sixfold coordinated with the oxygen forming an octahedral environment. The $(La_2O_2)^{2+}$ ions form a rocksalt-type substructure, where La is ninefold coordinated. This structure is coined K_2NiF_4 or "T-structure." The T-structure is characterized by the occupation of the apex position by oxygen. In the case of $Nd_{2-x}Ce_xCuO_4$, the $(Nd_2O_2)^{2+}$ ions form a fluorite-type sublattice, where Nd is eightfold coordinated. Consequently, Cu is fourfold coordinated forming square-planar CuO_2 planes. This structure is coined as the Nd_2CuO_4 or "T′-structure." The T′-structure is characterized by vacant apex sites. However, the apex site in T′-cuprates is the impurity position, and it is partially occupied in as-grown (AG) crystals. When superconductivity was first reported for electron-doped cuprates $Nd_{2-x}Ce_xCuO_4$,[1] it was known that a reduction process to the AG sample is vital for the induction of superconductivity. It is also well known that, the AG T′-cuprates are insulating antiferromagnets irrespective of the doping concentration.[2–16] Even though the microscopic origin of the role of the reduction process is still under intense debate,[17,18] the proximity of the antiferromagnetic (AF) and SC phases implies that the competition between the AF and SC states is strongly influenced during the reduction process. Richard *et al.*[19] have investigated AG $Pr_{1.85}Ce_{0.15}CuO_4$ by angle-resolved photoemission spectroscopy (ARPES) and found that AF order exists, resulting in an excitation edge gap along the nodal direction. However, after the application of a reduction process, the long-range AF order is suppressed, and the excitation gap is filled up. The appearance of such an excitation gap has been associated to AF interactions.[20] Hence, the reduction process does neither inject carriers nor modify the band dispersion in contrast to general assumptions. The SC dome in the electronic phase diagram might be considered as a consequence of the reduction process itself, i.e., the SC phase appears after a significant suppression of the Néel temperature and the disappearance of long-range AF order. So far, it was assumed that doping of electrons into the T′-cuprates is necessary for the induction of superconductivity. Already Brinkmann *et al.*[21] reported that modified annealing conditions for $Pr_{2-x}Ce_xCuO_4$ bulk samples results in an extended SC region, where superconductivity is observed at cerium concentrations as low as x = 0.04. Recently, Matsumoto *et al.*[22,23] have shown that T′-cuprates are SC even at x = 0.00. High SC transition temperatures at x = 0.00 have given rise to questions on the SC state, and hence, what the extra electrons are doing upon doping. While there have been a number of reports on the synthesis of dopant-free T′-cuprate superconductors,[23,24] to date there have been very limited investigations on the SC state. In this paper, we report on the transport, crystalline, and magnetization properties of optimally doped and dopant-free T′-$RE_{2-x}Ce_xCuO_4$ cuprates grown by molecular beam epitaxy (MBE).

II. EXPERIMENT AND SAMPLE PREPARATION

High-quality single-phase c axis-oriented thin films with a typical thickness of 100 nm of $La_{1.90}Ce_{0.10}CuO_4$, Pr_2CuO_4, $Pr_{1.86}Ce_{0.14}CuO_4$, Nd_2CuO_4, and $Nd_{1.85}Ce_{0.15}CuO_4$ have been grown by MBE on (001)$SrTiO_3$ substrates, whereas

(110)$YAlO_3$ substrates were used for $La_{1.91}Y_{0.09}CuO_4$ films.[23–27] Because our MBE setup is equipped with an electron impact emission spectroscopy sensor (EIES), the deposited cations are homogeneously distributed, i.e., we could not observe a noticeable doping gradient during the growth time. We used inductively coupled plasma analysis (ICP) on our samples to verify their stoichiometric composition independently. The ICP result well coincides with that of our EIES adjustment within 0.5% deviation. A small amount of Y^{3+} substitution is necessary to stabilize a dopant-free T′-$La_{1.91}Y_{0.09}CuO_4$ because T′-La_2CuO_4 films with high-crystalline quality could not be synthesized. $La_{1.90}Ce_{0.10}CuO_4$, $Pr_{1.86}Ce_{0.14}CuO_4$, $Nd_{1.85}Ce_{0.15}CuO_4$, and $La_{1.91}Y_{0.09}CuO_4$ films have been annealed (AN) *in situ* under ultrahigh vacuum (UHV) to induce superconductivity. For Pr_2CuO_4 and Nd_2CuO_4 films, an *ex situ* two-step annealing process was applied.[23] Electrical transport properties (standard four probe) between 300 and 1.8 K have been measured by using a 14 T physical property measurement system (PPMS), and the temperature-dependent magnetization data were recorded using a magnetic property measurement system (MPMS). High-resolution reciprocal space maps as well as symmetric diffraction patterns were measured with a Bruker D8 Advance four-circle x-ray diffractometer. The *c* and *a* axis lattice parameters are determined by applying a Nelson-Riley function to $2\theta/\omega$ diffraction patterns of the (0 0 2*l*) and (*h* 0 3*h*) diffraction planes, respectively.

III. RESULTS AND ANALYSIS

A. Normal state properties

Our AG cerium-doped and dopant-free T′-cuprate thin films are insulating.[25] Their resistivity values at 300 K are between 1.12 mΩcm for AG $La_{1.90}Ce_{0.10}CuO_4$ and 106 mΩcm for AG Nd_2CuO_4 (Table I). The resistivity values of Ce^{4+}-doped samples are smaller by a factor of five than their dopant-free analogs. After the annealing process, the resistivity value at 300 K dropped by a factor of 4.5 for $La_{1.90}Ce_{0.10}CuO_4$ and up to 170 for Nd_2CuO_4 films. We note that the change in resistivity after the annealing process for optimally doped T′-cuprates is typically smaller than that for dopant-free T′-cuprates. The *c* and *a* axis constants of AG and AN samples are given in Table I. In Figs. 1(a)–1(d), we show a crystallographic analysis for an AN-Pr_2CuO_4 thin film as an example. Generally, T′-cuprates are grown fully relaxed on (001)$SrTiO_3$ substrates [Fig. 1(a)] and therefore are not strained by the substrate lattice parameter. We did not observe any indications that the epitaxial relationship is modified by the annealing process. Equidistant stacking of CuO_2 planes as revealed by high-resolution transmission electron microscopy (HRTEM) images indicates that our films are free from unidentified phases, misorientations, or alternative stacking sequences [Fig. 1(b)]. Several reports suggest that the induction of superconductivity is associated with the appearance of $(RE,Ce)_2O_3$ sesquioxides, which appear during the reduction process, while Cu vacancies are filled, thus the resulting structure becomes stoichiometric.[28–32] However, our TEM data do not support such a scenario. In Fig. 1(c), the symmetric $2\theta/\omega$ diffraction spectrum of the AN-Pr_2CuO_4 thin film is plotted. A clear $(00\overline{14})$ reflection [Fig. 1(c)] together with a sharp rocking curve [full width half maximum (FWHM) = 0.11°, Fig. 1(d)] leave no doubt on a clean, single T′-phase film. We observed similar crystalline quality for our other T′-cuprate films. In agreement with earlier reports,[25] the *c* axis lattice constant of T′-cuprates decreases upon Ce^{4+} doping nearly linear according to Vegard's law[33] because the ionic radius of Ce^{4+} (0.97 Å) is smaller than that of La^{3+} (1.16 Å), Pr^{3+} (1.126 Å), or Nd^{3+} (1.109 Å).[34] On the other hand, the in-plane lattice constant *a* increases upon Ce^{4+} doping, a strong indication that the CuO_2 plane is doped

TABLE I. Crystallographic and electronic properties of the T′-cuprates investigated here, for AG as well as AN (Δ = 10 min, UHV) samples. The *c* and *a* axis lattice parameters are determined by applying a Nelson-Riley function to $2\theta/\omega$ scans of the (0 0 2*l*) and (*h* 0 3*h*) diffraction planes, respectively. Standard four-probe technique was used for measuring the resistivity values. The mean-free path is estimated for $\upsilon_F = 4.0 \cdot 10^5 \frac{m}{s}$ (Ref. 36), $m^* = m_e$, and σ_{ab} has been taken at 2 K. The Fermi temperature T_F was deduced from a nonlinear fit to$\rho(T) = \rho_0 + C(\frac{T}{T_F})^2 \ln(\frac{T_F}{T})$, where ρ_0 is the residual resistivity at 2 K and *C* a constant. The SC penetration depth λ was estimated by using the Homes relation $\rho_s \approx (120 \pm 25)\sigma_{ab}T_c$, where $\sigma_{ab} = 1/\rho(2K)$.

	$La_{1.90}Ce_{0.10}CuO_4$	$La_{1.91}Y_{0.09}CuO_4$	$Pr_{1.86}Ce_{0.14}CuO_4$	Pr_2CuO_4	$Nd_{1.85}Ce_{0.15}CuO$	Nd_2CuO_4
c axis (Å), AG	–	12.478 ± 0.001	12.202 ± 0.001	12.250 ± 0.001	12.090 ± 0.001	12.141 ± 0.001
c axis (Å), AN	12.457 ± 0.001	12.467 ± 0.001	12.148 ± 0.001	12.196 ± 0.001	12.082 ± 0.001	12.126 ± 0.001
a axis (Å), AG	–	4.023 ± 0.002	3.967 ± 0.002	3.964 ± 0.002	3.955 ± 0.002	3.940 ± 0.002
a axis (Å), AN	4.016 ± 0.002	4.022 ± 0.002	3.968 ± 0.002	3.959 ± 0.002	3.954 ± 0.002	3.941 ± 0.002
ρ(300 K) (mΩcm), AG	1.12 ± 0.06	5.73 ± 0.29	5.80 ± 0.24	31.0 ± 1.8	21.0 ± 1.1	114.0 ± 5.3
ρ(300 K) (mΩcm), AN	0.254 ± 0.01	0.442 ± 0.02	0.179 ± 0.01	0.302 ± 0.03	0.130 ± 0.007	0.670 ± 0.04
Annealing condition	500 °C, Δ	550 °C, Δ	630 °C, Δ	Two-step,[24]	630 °C, Δ	Two-step,[24]
T_c (K)	27.6 ± 0.1	22.0 ± 0.1	24.6 ± 0.1	25.1 ± 0.1	24.0 ± 0.1	24.9 ± 0.1
RRR = ρ(300 K)/ρ(30 K)	5.5	3.6	8.5	7.8	6.5	4.3
$\xi_{GL} = (\Phi_0/2\pi\mu_0 H_{c2})^{0.5}$ (nm)	5.9 ± 0.2	6.1 ± 0.3	6.4 ± 0.1	6.4 ± 0.1	6.8 ± 0.2	7.1 ± 0.3
ℓ (nm)	10.1 ± 0.2	6.7 ± 0.2	21.1 ± 0.2	6.3 ± 0.2	22.6 ± 0.2	2.9 ± 0.2
c in $\rho(T) = a+bT^c$	1.70 ± 0.05	1.63 ± 0.05	1.78 ± 0.05	1.77 ± 0.05	1.70 ± 0.05	1.50 ± 0.05
$n(10^{20}$ cm$^{-3})$	23.9 ± 1.7	3.45 ± 0.5	124 ± 19	28.0 ± 4.2	28.6 ± 4.5	3.52 ± 0.5
T_F (K)	7573 ± 325	2082 ± 15.4	22673 ± 709	8396 ± 274	8527 ± 290	2109 ± 23
λ (nm)	188 ± 40	275 ± 55	134 ± 27	180 ± 36	132 ± 27	364 ± 73

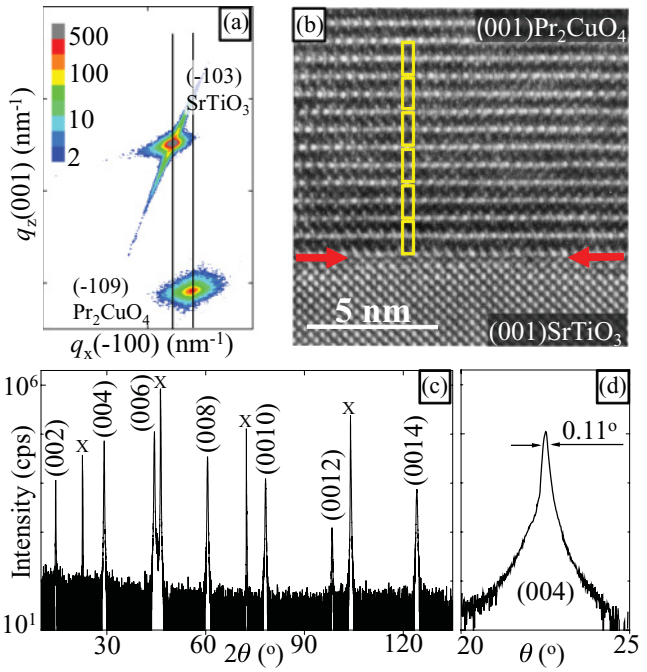

FIG. 1. (Color online) Typical structural properties of SC Pr_2CuO_4 thin films grown on (001)$SrTiO_3$ substrates. (a) Reciprocal space map (RSM) of the (−109) diffraction peak of Pr_2CuO_4 ($-2.8\ \mathrm{nm}^{-1} \leqslant q_x \leqslant -2.4\ \mathrm{nm}^{-1}$ and $7.3\ \mathrm{nm}^{-1} \leqslant q_z \leqslant 8.0\ \mathrm{nm}^{-1}$). (b) HRTEM image of the interface region (marked by arrows). The boxes indicate single-unit cell dimensions. (c) $2\theta/\omega$ x-ray diffraction. The diffraction peaks of the Pr_2CuO_4 film and substrate material are marked by their (*hkl*) multiplicity and x, respectively. (d) Rocking curve of (004) diffraction peak.

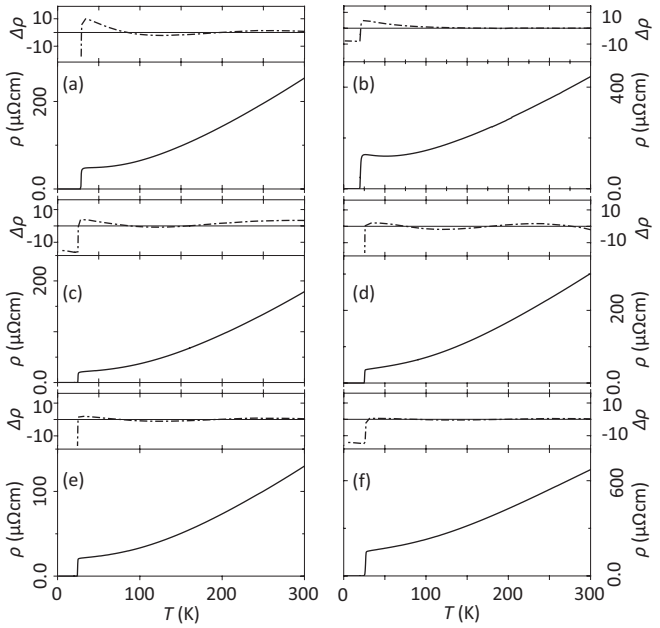

FIG. 2. The temperature dependence of the resistivities for (a) AN-$La_{1.90}Ce_{0.10}CuO_4$, (b) AN-$La_{1.91}Y_{0.09}CuO_4$, (c) AN-$Pr_{1.86}Ce_{0.14}CuO_4$, (d) AN-Pr_2CuO_4, (e) $Nd_{1.85}Ce_{0.15}CuO_4$, and (f) AN-Nd_2CuO_4 are shown. Above each graph, we plot the deviation resistivity $\Delta\rho = \rho(\mathrm{T})\text{-}\rho_{\mathrm{fit}}$ (T) as a function of temperature, where $\rho_{\mathrm{fit}}(T) = \rho_0 + C(\frac{T}{T_F})^2 \ln(\frac{T_F}{T})$ (see Table I). The fitting range was 100–400 K and 40–300 K for (a) and (b)–(f), respectively.

by electrons. A notable change of the *c* axis length for AG and AN samples points to a substantial rearrangement of the oxygen occupancies. Early neutron scattering data have shown that a certain amount of oxygen, located preferentially at the apical position, leave the crystal, resulting in shrinkage of the *c* axis length.[16] However, the in-plane lattice constants *a* appear to be independent of the annealing process, as it remains constant within experimental deviations. This is a remarkable correlation as it provides an additional hint that the reduction process is, unlike Ce^{4+} doping, not associated to the doping of electrons into the CuO_2 planes. After the annealing process, the resistivity value at 300 K decreases, and moreover, the temperature dependences of our T′-cuprates do not behave like insulators anymore, but metals. An often used criteria of a superior crystalline quality is the residual resistivity ratio (RRR): $\mathrm{RRR} = \frac{\rho_{300K}}{\rho_{30K}}$, i.e., larger RRR values represent better crystalline qualities. In Figs. 2(a)–2(f), we show the in-plane resistivity curves $\rho_{ab}(T)$ for $La_{1.90}Ce_{0.10}CuO_4$, $La_{1.91}Y_{0.09}CuO_4$, $Pr_{1.86}Ce_{0.14}CuO_4$, Pr_2CuO_4, $Nd_{1.85}Ce_{0.15}CuO_4$, and Nd_2CuO_4 after annealing. Although the absolute resistivity values increase from La to Nd, all of our samples are metallic, and the RRR values are between 3.6 and 8.5 for AN-$La_{1.91}Y_{0.09}CuO_4$ and AN-$Pr_{1.86}Ce_{0.14}CuO_4$, respectively. Such large RRR values for T′-cuprates have not been observed even for single crystals, and limited reports are available for optimally doped $Pr_{1.86}Ce_{0.14}CuO_4$.[35] As we already pointed out, T′-cuprates with optimal doping levels show lower resistivity values than dopant-free T′-cuprate superconductors. Unlike the linear dependence observed for hole-doped cuprates, such as $YBa_2Cu_3O_7$, the normal state resistivity of T′-cuprates is close to a T^2 dependence which suggests a Fermi liquid behavior. A fit to the temperature-dependent resistivity with $\rho(T) = a + b \cdot T^c$ between 300 and 30 K results in $c \approx 1.77$ and $c \approx 1.78$ for AN-Pr_2CuO_4 and AN-$Pr_{1.86}Ce_{0.14}CuO_4$, respectively. Also, in the case of AN-$La_{1.90}Ce_{0.10}CuO_4$ and AN-$La_{1.91}Y_{0.09}CuO_4$, the *c* values are similar (Table I). In the case of AN-$Nd_{1.85}Ce_{0.15}CuO_4$ and AN- Nd_2CuO_4, the deviation is larger. The general deviation to the T^2 dependence may be explained in that the T^2 relation is deduced from a three-dimensional (3D) Fermi liquid, whereas the T′-cuprates represent a two-dimensional (2D) system. A commonly used expression for 2D Fermi liquid systems is[36] $\rho(T) = \rho_0 + C(\frac{T}{T_F})^2 \ln(\frac{T_F}{T})$, where ρ_0 is the residual resistance, *C* a constant, and T_F is the Fermi temperature. We used *C* and T_F as fitting parameters to our experimental data, and the results are given in Table I. We derived the Fermi temperature T_F by assuming that the electrons are distributed in a box with infinite walls. The charge-carrier concentration *n* is $n = \int_0^\infty f(E)D(E)dE$, where $f(E)$ is the occupation probability and $D(E)$ the density of energy states. When $T \to 0$ K, the Fermi temperature can be correlated to the charge-carrier density *n* as follows: $T_F = \frac{\hbar^2(3\pi^2 n)^{2/3}}{2mk_B}$, where *m* is the electron mass. Our approximation may reflect the trend of the carrier concentration, although for a more thorough investigation, appropriate $f(E)$ and $D(E)$ for 2D systems should be considered. For optimally doped samples, we expect larger *n* than for dopant-free samples. From the *n* values given in Table I, one can see that optimally doped samples show larger *n* values than their dopant-free

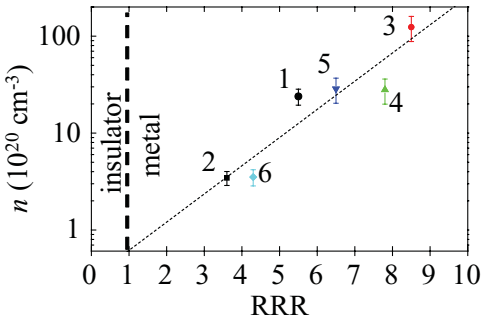

FIG. 3. (Color online) The deduced charge-carrier concentration n as a function of the residual resistivity ratio RRR $= \rho(300\,\mathrm{K})/\rho(30\,\mathrm{K})$ of (1) AN-$La_{1.90}Ce_{0.10}CuO_4$, (2) AN-$La_{1.91}Y_{0.09}CuO_4$, (3) AN-$Pr_{1.86}Ce_{0.14}CuO_4$, (4) AN-Pr_2CuO_4, (5) AN-$Nd_{1.85}Ce_{0.15}CuO_4$, and (6) AN-Nd_2CuO_4. The short dashed line is a linear interpolation of the data points. For RRR<1, a system is considered to be an insulator. The crossover from a metallic into an insulating state appears for $n \approx 0.61 \times 10^{20}\mathrm{cm}^{-3}$.

analogs. For AN-$Pr_{1.86}Ce_{0.14}CuO_4$, the fitting process led to a Fermi temperature of approximately 23 000 K, resulting in a charge-carrier concentration$n \approx 1.25 \times 10^{22}$ cm^{-3}. This carrier concentration is 4.5 times larger than that of AN-Pr_2CuO_4, which is very close to that obtained by Hall effect measurements.[22] In the La-based T′-cuprates, the Ce doping increases n by a factor of 7, whereas it is more than eight times for the Nd-based cuprates. We cautiously note that the obtained values for the Fermi temperatures T_F, and thereby the charge-carrier concentration n, significantly depend on the temperature fitting range. Here, the temperature-dependent resistivity data have been fitted between 50 and 300 K. For a fitting range of 40 to 300 K, the Fermi temperature typically increases, e.g., for AN-Nd_2CuO_4 from 2109 K up to 2632 K. Also, the one order of magnitude deviation of T_F (Table I) between materials with identical crystal structure may arise from a difference of the sample quality. For example, the T_F of AN-$Nd_{1.85}Ce_{0.15}CuO_4$ is estimated to be approximately 8500 K for our samples, whereas it was reported to be 3000 K,[36] most likely due to differences in sample quality. As we used a 3D model of the Fermi temperature, however, n is merely influenced. Nonetheless, a 3D electron system is a crude approximation for the T′-cuprates as the 2D nature of the electronic density of states (DOS) has been ignored.[52] In Fig. 3, we plot the charge-carrier density n as a function of the RRR values for T′-cuprates. A least-square linear fit indicates a metal-insulator transition for $n_{\mathrm{MIT}} \approx 0.61 \times 10^{20}$ cm^{-3}. The large RRR values are correlated to high conductivity values at low temperatures. Such a correlation might be used to estimate the mean-free path ℓ by using $\frac{hd\sigma_{ab}}{e^2} = k_F\ell$. Here, d is the distance between CuO_2 planes, σ_{ab} is the in-plane conductivity, and e is the charge of an electron. An upper limit of ℓ can be obtained by estimating the Fermi wave number, $k_F \cong \frac{mv_F}{\hbar}$ using m as the bare electron mass and v_F from photoemission measurements ($v_F \approx 4.0 \times 10^5$ m/s).[37] We caution that m might deviate[38] from the free-electron mass. Actually, by adopting the T_F value for AN-$Pr_{1.86}Ce_{0.14}CuO_4$ (≈23 000 K), the effective mass m^* was estimated to be 4.3 m using $T_F = \frac{m^*}{2k_B}v_F^2$. As shown in Table I, ℓ significantly decreases from cerium-doped to dopant-free T′-cuprates. While ℓ corresponds to approximately 57 unit cells for optimally doped $Nd_{1.85}Ce_{0.15}CuO_4$, it is less than 8 unit cells for dopant-free Nd_2CuO_4. The residual conductivity σ_{ab} is the dominating factor of ℓ and typically smaller for dopant-free T′-cuprates. It is likely that ℓ is affected by the interconnection of the crystal grains and the spatial inhomogeneity of oxygen defects as the two-step annealing process may have a strong impact on ℓ. Therefore, we remain skeptical to assign the smaller value of ℓ as an intrinsic property to square-planar-coordinated cuprates with lower doping levels. Actually, the reported ℓ value of 2.7 nm by Dagan *et al.*[39] for $Pr_{1.85}Ce_{0.15}CuO_4$ grown by pulsed laser deposition (PLD) technique is significantly smaller than our value of $\ell = 21.1$ nm, which indicates that ℓ is a sensitive measure of the crystallinity and microstructure.

B. Properties of the SC state

The utmost striking difference between AG- and AN-T′-cuprates is that the AN-T′-cuprates are superconductors. We would like to emphasize the importance of a fine-tuned annealing process, which significantly depends on the Ce doping level x. For optimal doping levels, a vacuum annealing process is sufficient to induce superconductivity, whereas for dopant-free T′-cuprates, a two-step annealing process is required to induce superconductivity. The SC transition temperatures, taken from $\rho(T)$measurements, of our AN-T′-cuprates are given in Table I. While AN-$Nd_{1.85}Ce_{0.15}CuO_4$ becomes SC at 24.0 K, it is 24.9 K for the dopant-free AN-Nd_2CuO_4. A similar behavior is observed for Pr-based samples, where the T_c's are 24.6 and 25.1 K for the optimally doped and dopant-free cuprate, respectively. However, for La-based cuprates, this is not the case, as T_c is higher for the optimally doped cuprate. A reasonable explanation for this behavior lies beneath the T′-structure itself. It is well known that the T′-cuprates with La cannot be grown as single crystals or bulk powder, as the competing T-structure is the favorable structure due to the temperature-dependent tolerance factor.[40] In the present investigation, however, the films are synthesized by MBE, where the synthesis temperature is significantly lower than that in bulk synthesis. Nonetheless, the growth of high-quality T′-La_2CuO_4 films remains a challenging task even by MBE.[41] The substitution of large La^{3+} ions by smaller rare earth ions significantly promotes the stabilization of the T′-phase. Therefore, we added a small amount of Y^{3+} to stabilize high-quality T′-cuprate thin films. Because Y^{3+} is smaller than La^{3+} ions, the c axis is smaller than that of T′-La_2CuO_4. In Fig. 4, the SC phase diagram of 217 samples of T′-$La_{2-x}Ce_xCuO_4$ films is shown. At $x_{\mathrm{Ce}} \approx 0.09$, T_c is highest. For smaller x_{Ce}, T_c rapidly decays as the competition between the T- and T′- structure increases. The threshold for the Cerium-doped T′-structure is at x_{crit} ≈0.06, and the films crystallize in the T-structure for smaller cerium concentrations. In the absence of such a structural instability, T_c may still increase for smaller doping levels. Therefore, we speculate, that a single-phase T′-La_2CuO_4 film gives a higher T_c than our present AN-$La_{1.91}Y_{0.09}CuO_4$.

The SC transition observed from our transport measurements might be a consequence of crystalline inhomogenities, or it may appear only at the surface or interface region of

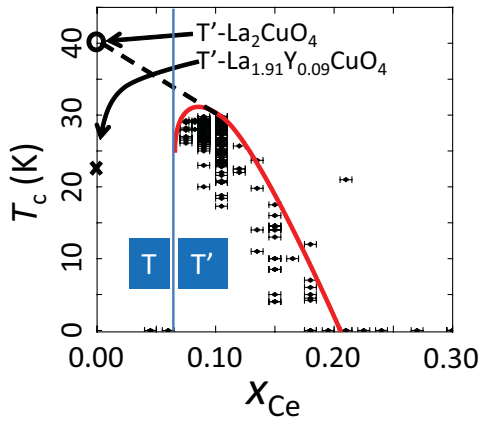

FIG. 4. (Color online) The SC phase diagram of 217 T′-$La_{2-x}Ce_xCuO_4$ films grown on (001) $SrTiO_3$ substrates is shown as a function of the Ce doping level x_{Ce}. The solid line (red) is a guide to the eye. For $x < x_{crit} \approx 0.06$, the crystal structure changes from T′ to T structure. At $x = 0.00$, we stabilized the T′-structure by a small amount of Y (cross). The dashed line is an extrapolation of the SC region towards the undoped compound T′-La_2CuO_4 (circle).

the sample. While crystalline inhomogenities (Fig. 1) have been ruled out, surface- or interface-related superconductivity may still exist. However, if such a SC state is realized in our samples, the diamagnetic response would be significantly smaller than the detection limitations.[42] In Figs. 5(a) and 5(b), we show the temperature-dependent magnetic moment recorded under zero-field-cooled (ZFC) and field-cooled cooling (FCC) conditions for optimally doped and dopant-free T′-cuprate superconductors, respectively. All of our magnetization measurements were carried out with the film planes oriented parallel to the external magnetic field (10 Oe), thus, additional corrections for the demagnetization factor are not required.[43] In Fig. 5(a), the diamagnetic signals at 2 K detected

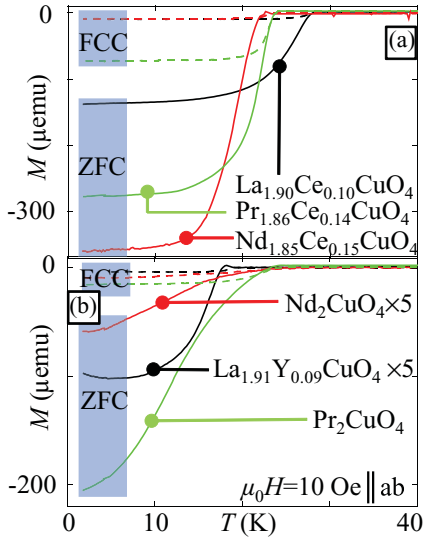

FIG. 5. (Color online) Magnetization as a function of temperature of optimally doped samples (a) and dopant-free samples (b). An external magnetic field of 10 Oe is applied parallel to the film surface. Solid and dashed lines correspond to ZFC and FCC procedures, respectively.

for optimally doped T′-cuprates are -0.14×10^{-3} emu (≈ -14 emu/cm^3) and -0.39×10^{-3} emu (≈ -39 emu/cm^3) for AN-$La_{1.90}Ce_{0.10}CuO_4$ and AN-$Nd_{1.85}Ce_{0.15}CuO_4$ films, respectively, in ZFC mode. At first sight, this result might be somewhat surprising, as one may expect a stronger diamagnetic response for AN-$La_{1.90}Ce_{0.10}CuO_4$ due to its higher T_c. However, as we will see later, this result is a consequence of a smaller superfluid density n_s in the SC state when compared to Pr- or Nd-based T′-cuprates. Nonetheless, comparable data in literature remain elusive, thus supporting our superior sample quality. Strong vortex pinning forces[44] result in a reduced diamagnetic response observed in FCC mode. Moreover, the thickness of our films of 100 nm is significantly smaller than reported SC penetration depth values obtained by microwave absorption experiments.[45,46] We did not develop a sophisticated model to simulate the SC volume fraction of our films. Instead, we determined the SC volume fraction directly from the magnetization value measured under FCC conditions. For optimally doped T′-cuprates, a SC volume fraction of 28% was estimated. In Fig. 5(b), the diamagnetic signals at 2 K detected for dopant-free T′-cuprates are -0.21×10^{-3} emu (≈ -21 emu/cm^3) and -0.02×10^{-3} emu (≈ -2 emu/cm^3) for AN-Pr_2CuO_4 and AN- Nd_2CuO_4, respectively, in ZFC mode. While the diamagnetic response of AN-Pr_2CuO_4 is comparable to that of AN- $Pr_{1.85}Ce_{0.15}CuO_4$, it is much smaller for AN- Nd_2CuO_4 and AN-$La_{1.91}Y_{0.09}CuO_4$. For AN-Pr_2CuO_4 we estimated a SC volume fraction of 19% by using the FCC data. For AN- Nd_2CuO_4 and AN-$La_{1.91}Y_{0.09}CuO_4$ the SC volume fraction is about 3%. Again, also for those values, one has to take into account that λ is much larger than the film thickness and that flux pinning plays a crucial role for the overall detected diamagnetic signal strengths.

A very important parameter of a superconductor is the SC coherence length ξ_{GL}, as it determines on what length scales the Cooper pairing takes place. In the present case we determined ξ_{GL} from the upper critical magnetic field H_{c2} at 1.8 K, determined from resistivity measurements. In contrast to our magnetization measurements, the films are aligned perpendicular to the external magnetic field. Resistivity measurements are "acceptable" for the determination of H_{c2} since Nernst effect measurements and theoretical considerations[47] have shown that H_{c2} corresponds indeed to the upper limit of the pair-breaking field. In principal, H_{c2} should be determined at $T \ll T_c$, which is the case in our present experiment. The absolute value of H_{c2} was determined from the $\rho(B)$ curves at 1.8 K, when the resistivity value is 10% below its normal state value. A similar analysis was done for $\rho(B)$ curves at different temperatures as well as $\rho(T)$ curves taken under different magnetic fields. For the preparation of the thermodynamic SC phase diagrams, we assumed that $\frac{\partial H_{c2}}{\partial T_c}|_{T=0K} = 0$ (Fig. 6). Although the doping concentration level is completely different, the thermodynamic SC phase diagrams overlap each other for Nd- and Pr-based cuprates. As we have mentioned earlier, using Y in La-based T′-cuprates simply promotes the stability of the T′-phase. T_c is lower, but H_{c2} reaches nearly the same value for optimally doped and dopant-free La-based T′-cuprate superconductors. In Fig. 7, we plot the $\rho(B)$ curves for all samples discussed here. For clarity reasons, the absolute resistivity values have

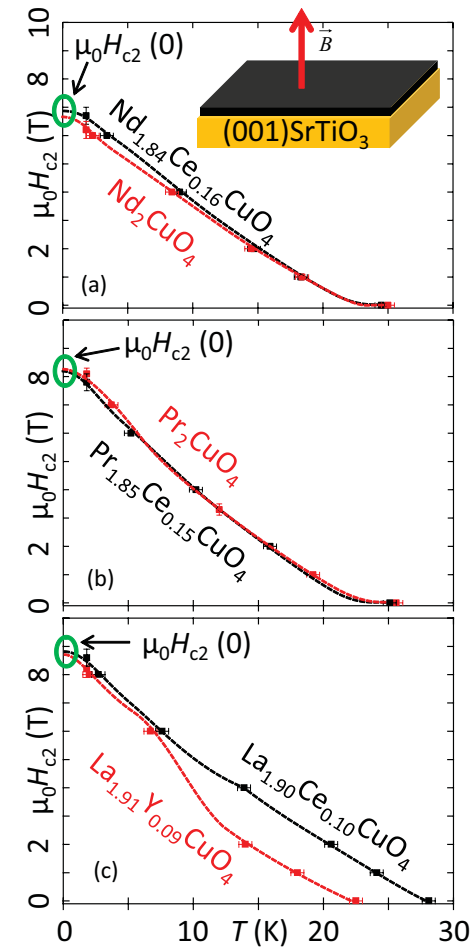

FIG. 6. (Color online) The thermodynamic SC phase diagrams for (a) Nd-based, (b) Pr-based, and (c) La-based T′-cuprates are plotted. At $T = 0$ K, we assumed that $\frac{\partial H_{c2}}{\partial T_c}|_{T=0K} = 0$. The data points have been derived from electrical transport measurements, where the criteria for the H_{c2} value was that the resistance is 10% below its normal state value.

been normalized to 14 T. The H_{c2} values are highest for La-based T′-cuprates, and there appears to be no significant doping dependence. The influence of doping on H_{c2} in the case of AN-Pr_2CuO_4 and AN-$Pr_{1.85}Ce_{0.15}CuO_4$ is within experimental error bars negligible as both $\rho(B)$ curves show an identical transition behavior. In the La-based T′-cuprates, the transition of AN-$La_{1.91}Y_{0.09}CuO_4$ appears to be broader than that of AN-$La_{1.90}Ce_{0.10}CuO_4$. Nonetheless, in both cases, the transition ends almost at the same field. In the case of Nd-based cuprates, a small deviation between optimally doped and dopant-free cuprates are observed. The very reason for that behavior remains unclear at present.

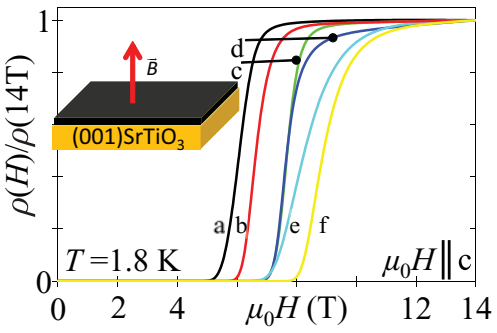

FIG. 7. (Color online) The normalized magneto resistance in plotted for (a) AN-Nd_2CuO_4, (b) AN-$Nd_{1.85}Ce_{0.15}CuO_4$, (c) AN-Pr_2CuO_4, (d) AN-$Pr_{1.86}Ce_{0.14}CuO_4$, (e) AN-$La_{1.91}Y_{0.09}CuO_4$, and (f) AN-$La_{1.90}Ce_{0.10}CuO_4$. The external magnetic field was applied perpendicular to the film plane. The resistivity was normalized at 14 T.

IV. DISCUSSIONS

The universal relation provided by Homes *et al.*[48] for superconductors in general $(\omega_p^2 \approx (120 \pm 25)\sigma_{ab}T_c)$ shows that the superfluid density $n_s = \frac{m\omega_p^2}{4\pi e^2}$ is proportional to the product of the in-plane conductivity σ_{ab} at T_c and T_c itself, where ω_p is the SC plasma frequency. Together with $\lambda^2 = \frac{m}{4\pi n_s e^2}$ and $4\pi\lambda^2\mu_0 H_{c1} = \phi_0(\ln\lambda - \ln\xi_{GL})$, we estimated the penetration depths of our T′-cuprate superconductors (Table I). Within the limits given by the Homes relation, for optimally doped T′-cuprates, our estimated penetration depths coincide well with reported experimental data.[45,46] Therefore, our estimations for the dopant-free T′-cuprates may be reasonable approximations. In Fig. 8, we plotted T_c as a function of n and λ^{-2}. A clear correlation between the charge-carrier density and T_c may not be traced. Although n is always larger for optimally doped T′-cuprates, it does not influence T_c. Also, a larger value of λ^{-2} has no influence on the pairing interaction. Instead, T_c appears to be rather independent on n and/or n_s, and a critical doping level is not a prerequisite for the induction of superconductivity into T′-cuprates. In Fig. 9, ξ_{GL} is plotted as a function of the unit cell lattice parameters of T′-cuprates. ξ_{GL} becomes smaller for larger a and c axis lengths, a strong indication that T′-cuprates with larger unit cell lattice parameters are closer to 2D superconductors. We also expect a relation between T_c and ξ_{GL} because T′-cuprates with larger RE give higher T_c values. In our study, AN-$La_{1.91}Y_{0.09}CuO_4$ might be considered as an exceptional case, as T_c is significantly lower than that

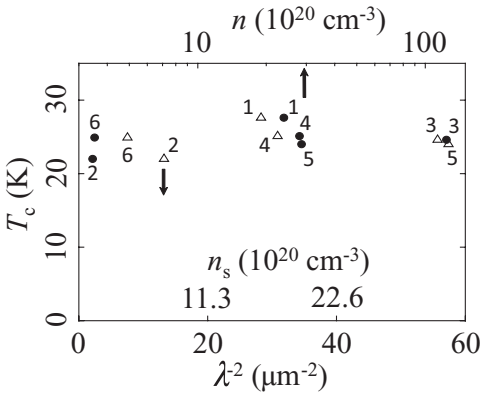

FIG. 8. The SC transition temperature T_c as a function of λ^{-2} (triangle: lower axis) and the charge-carrier concentration n (dot: upper axis) for (1) AN-$La_{1.90}Ce_{0.10}CuO_4$, (2) AN-$La_{1.91}Y_{0.09}CuO_4$, (3) AN-$Pr_{1.86}Ce_{0.14}CuO_4$, (4) AN-Pr_2CuO_4, (5) AN-$Nd_{1.85}Ce_{0.15}CuO_4$, and (6) AN-Nd_2CuO_4.

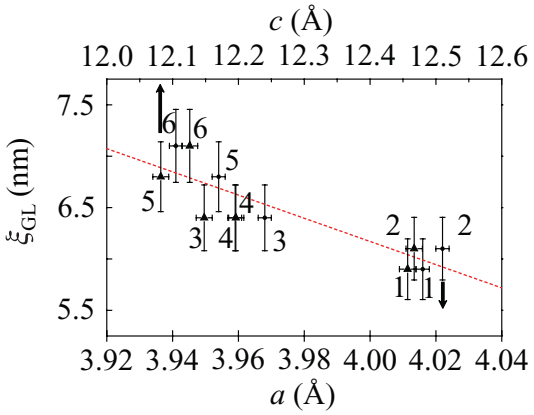

FIG. 9. (Color online) The SC coherence length ξ_{GL} as a function of the in-plane lattice constant a (dot: lower axis) and the c axis length (triangle: upper axis) are plotted for (1) AN-$La_{1.90}Ce_{0.10}CuO_4$, (2) AN-$La_{1.91}Y_{0.09}CuO_4$, (3) AN-$Pr_{1.86}Ce_{0.14}CuO_4$, (4) AN-Pr_2CuO_4, (5) $Nd_{1.85}Ce_{0.15}CuO_4$, and (6) AN-Nd_2CuO_4. The short dashed line is a linear fit to the data points.

of optimally doped AN- $La_{1.90}Ce_{0.10}CuO_4$. At present we speculate that a SC T′-La_2CuO_4 cuprate will follow this trend.

V. CONCLUSIONS

In summary, we have synthesized SC T′-$RE_{2-x}Ce_xCuO_4$ (RE = La, Pr, Nd) thin films by MBE at optimal as well as $x = 0.00$ doping levels. Our analysis shows that irrespective of the doping level, the appearance of superconductivity seems to be a universal phenomenon in T′-cuprates. The fact that doping does not alter the SC ground state in T′-cuprates deserves further considerations because it is in strong contrast to hole-doped cuprates. Recent theoretical considerations[49,50] suggest that a Slater-insulating ground state is favorable for T′-cuprates raising further doubt on the common prejudged Mott-insulating and AF ground state. We further demonstrated by magnetization measurements that a bulklike SC response is observed for T′-cuprate superconductors over a wide range of the electronic phase diagram, including $x = 0.00$. At the present stage we might not be able to clarify the impact of the extra doped electrons on the electronic structure with respect to dopant-free T′-cuprates as the SC instability of the Fermi surface seems to be related to Cu-O bond lengths. A careful analysis of the Hall coefficient[51] might be a useful tool for a deeper understanding of the charge-carrier correlations on the Fermi topology. The overt asymmetry between electron- and hole-doped cuprates calls for further theoretical and experimental investigations.

ACKNOWLEDGMENT

The authors are grateful for the efforts taken by Y. Sekine supporting magnetic transport measurements.

*yoshiharu.k@lab.ntt.co.jp
†Present address: Department of Applied Physics, Tokyo University of Science, 1-3 Kagurazaka, Shinjuku, Tokyo 162-8601, Japan.
‡On leave from Nagaoka University of Technology.

[1] Y. Tokura, H. Takagi, and S. Uchida, Nature (London) **337**, 345 (1989).
[2] M. P. Allenspach, S. W. Choeng, A. Dommann, P. Fischer, Z. Fisk, A. Furrer, H. R. Ott, and B. Rupp, Z. Phys. B **77**, 185 (1989).
[3] M. Matsuda, K. Yamada, K. Kakurai, H. Kadowaki, T. R. Thurston, Y. Endoh, Y. Hidaka, R. J. Birgeneau, M. A. Kastner, P. M. Gehring, A. H. Moudden, and G. Shirane, Phys. Rev. B **42**, 10098 (1990).
[4] D. E. Cox, A. I. Goldman, M. A. Subramanian, J. Gopalakrishnan, and A. W. Sleight, Phys. Rev. B **40**, 6998 (1989).
[5] I. W. Sumarlin, J. W. Lynn, T. Chattopadhyay, S. N. Barilo, D. I. Zhigunov, and J. L. Peng, Phys. Rev. B **51**, 5824 (1995).
[6] H. Casalta, P. Bourges, M. d'Astuto, D. Petitgrand, and A. Ivanov, Phys. Rev. B **57**, 471 (1998).
[7] K. Berggold, T. Lorenz, J. Baier, M. Kriener, D. Senff, H. Roth, A. Severing, H. Hartmann, A. Freimuth, S. Barilo, and F. Nakamura, Phys. Rev. B **73**, 104430 (2006).
[8] T. Chattopadhyay, J. W. Lynn, N. Rosov, T. E. Grigereit, S. N. Barilo, and D. I. Zhigunov, Phys. Rev. B **49**, 9944 (1994).
[9] J. D. Thompson, S.-W. Cheong, S. E. Brown, Z. Fisk, S. B. Oseroff, M. Tovar, D. C. Vier, and S. Schultz, Phys. Rev. B **39**, 6660 (1989).
[10] P. W. Klamut, Phys. Rev. B **50**, 13009 (1994).
[11] Y. Endoh, M. Matsuda, K. Yamada, K. Kakurai, Y. Hidaka, G. Shirane, and R. J. Birgeneau, Phys. Rev. B **40**, 7023 (1989).
[12] S. Skanthakumar, J. W. Lynn, J. L. Peng, and Z. Y. Li, Phys. Rev. B **47**, 6173 (1993).
[13] I. A. Zobkalo, A. G. Gukasov, S. Yu, A. Kokovin, S. N. Barilo, and D. I. Zhigunov, Solid State Commun. **80**, 921 (1991).
[14] S. Skanthakumar, J. W. Lynn, J. L. Peng, and Z. Y. Li, J. Appl. Phys. **73**, 6326 (1993).
[15] R. Hord, H. Luetkens, G. Pascua, A. Buckow, K. Hofmann, Y. Krockenberger, J. Kurian, H. Maeter, H.-H. Klauss, V. Pomjakushin, A. Suter, B. Albert, and L. Alff, Phys. Rev. B **82**, 180508R (2010).
[16] M. Matsuda, Y. Endoh, K. Yamada, H. Kojima, I. Tanaka, R. J. Birgeneau, M. A. Kastner, and G. Shirane, Phys. Rev. B **45**, 12548 (1992).
[17] N. P. Armitage, P. Fournier, and R. L. Greene, Rev. Mod. Phys. **82**, 2421 (2010).
[18] M. Imada, A. Fujimori, and Y. Tokura, Rev. Mod. Phys. **70**, 1039 (1998).
[19] P. Richard, M. Neupane, Y. M. Xu, P. Fournier, S. Li, P. Dai, Z. Wang, and H. Ding, Phys. Rev. Lett. **99**, 157002 (2007).
[20] A. A. Kordyuk, S. V. Borisenko, M. Knupfer, and J. Fink, Phys. Rev. B **67**, 064504 (2003).
[21] M. Brinkmann, T. Rex, H. Bach, and K. Westerholt, Phys. Rev. Lett. **74**, 4927 (1995).
[22] O. Matsumoto, A. Utsuki, A. Tsukada, H. Yamamoto, T. Manabe, and M. Naito, Phys. Rev. B **79**, 100508(R) (2009).

[23]H. Yamamoto, Y. Krockenberger, and M. Naito, Solid State Commun. **151**, 771 (2011).
[24]Y. Krockenberger, H. Yamamoto, M. Mitsuhashi, and M. Naito, Jpn. J. Appl. Phys. **51**, 010106 (2012).
[25]A. Tsukada, M. Noda, H. Yamamoto, and M. Naito, Physica C **426-431**, 459 (2005).
[26]Y. Krockenberger, J. Kurian, A. Winkler, A. Tsukada, M. Naito, and L. Alff, Phys. Rev. B **77**, 060505R (2008).
[27]M. Naito, S. Karimoto, and A. Tsukada, Supercond. Sci. Technol. **15**, 1663 (2002).
[28]E. Wang, J. M. Tarascon, L. H. Greene, G. W. Hull, and W. R. McKinnon, Phys. Rev. B **41**, 6582 (1990).
[29]P. Dai, H. J. Kang, H. A. Mook, M. Matsuura, J. W. Lynn, Y. Kurita, S. Komiya, and Y. Ando, Phys. Rev. B **71**, 100502 (2005).
[30]H. J. Kang, P. Dai, B. J. Campbell, P. J. Chupas, S. Rosenkrantz, P. L. Lee, Q. Huang, S. Li, S. Komiya, and Y. Ando, Nat. Mater. **6**, 224 (2007).
[31]M. Matsuura, P. Dai, H. J. Kang, J. W. Lynn, D. N. Argyriou, K. Prokes, Y. Onose, and Y. Tokura, Phys. Rev. B **68**, 144503 (2003).
[32]K. Kurahashi, H. Matsushita, M. Fujita, and K. Yamada, J. Phys. Soc. Jpn. **71**, 910 (2002).
[33]L. Vegard, Z. Physik **5**, 17 (1921).
[34]R. D. Shannon, Acta Crystallogr. A **32**, 751 (1976).
[35]G. Roberge, S. Charpentier, S. Goudin-Proulux, P. Rauwel, K. D. Truong, and P. Fournier, J. Cryst. Growth **311**, 1340 (2009).
[36]C. C. Tsuei, A. Gupta, and G. Koren, Physica C **161**, 415 (1989).
[37]N. P. Armitage, D. H. Lu, C. Kim, A. Damascelli, K. M. Shen, F. Ronning, D. L. Feng, P. Bogdanov, X. J. Zhou, W. L. Yang, Z. Hussain, P. K. Mang, N. Kaneko, M. Greven, Y. Onose, Y. Taguchi, Y. Tokura, and Z. X. Shen, Phys. Rev. B **68**, 064517 (2003).
[38]C. C. Homes, B. P. Clayman, J. L. Peng, and R. L. Greene, Phys. Rev. B **56**, 5525 (1997).
[39]Y. Dagan, R. Beck, and R. L. Greene, Phys. Rev. Lett. **99**, 147004 (2007).
[40]J. F. Bringley, S. S. Trail, and B. A. Scott, J. Solid State Chem. **88**, 590 (1990).
[41]H. Yamamoto, O. Matsumoto, A. Tsukada, and M. Naito, Physica C **470**, 1025 (2010).
[42]M. E. Huber, M. C. Koshnick, H. Bluhm, L. J. Archuleta, T. Azua, P. G. Bjornsson, B. W. Gardner, S. T. Halloran, E. L. Lucero, and K. A. Moler, Rev. Sci. Instrum. **79**, 053704 (2008).
[43]C. P. Bean, Phys. Rev. Lett. **8**, 250 (1962).
[44]Y. Zuev, T. R. Lemberger, J. A. Skinta, T. Greibe, and M. Naito, Phys. Status Solidi B **236**, 412 (2003).
[45]J. A. Skinta, M.-S. Kim, T. R. Lemberger, T. Greibe, and M. Naito, Phys. Rev. Lett. **88**, 207005 (2002).
[46]J. R. Cooper, Phys. Rev. B **54**, 3753 (1996).
[47]A. Hackl and S. Sachdev, Phys. Rev. B **79**, 235124 (2009).
[48]C. C. Homes, S. V. Dordevic, M. Strongin, D. A. Bonn, R. Liang, W. N. Hardy, S. Komiya, Y. Ando, G. Yu, N. Kaneko, X. Zhao, M. Greven, D. N. Basov, and T. Timusk, Nature (London) **430**, 539 (2004).
[49]C. Weber, K. Haule, and G. Kotliar, Nat. Physics **6**, 574 (2010).
[50]H. Das and T. Saha-Dasgupta, Phys. Rev. B **79**, 134522 (2009).
[51]N. P. Ong, Phys. Rev. B **43**, 193 (1991).
[52]S. Das Sarma, V. M. Galitski, and Y. Zhang, Phys. Rev. B **69**, 125334 (2004).